ACS APPLIED MATERIALS & INTERFACES

Research Article

Cite This: ACS Appl. Mater. Interfaces 2019, 11, 47153−47161

www.acsami.org

Motion-Programmed Bar-Coating Method with Controlled Gap for High-Speed Scalable Preparation of Highly Crystalline Organic Semiconductor Thin Films

Seon Baek Lee,[†,∥] Boseok Kang,[†,‡,∥] Daegun Kim,[†] Chaneui Park,[†] Seulwoo Kim,[§] Minhwan Lee,[§] Won Bo Lee,[§] and Kilwon Cho*[,†]

[†]Department of Chemical Engineering and Center for Advanced Soft Electronics, Pohang University of Science and Technology, 77 Cheongam-Ro, Nam-gu, Pohang 37673, Korea

[‡]SKKU Advanced Institute of Nanotechnology and Department of Nano Engineering, Sungkyunkwan University (SKKU), Suwon 16419, Korea

[§]School of Chemical and Biological Engineering, Seoul National University, 1 Gwanak-Ro, Gwanak-gu, Seoul 08826, Korea

Supporting Information

ABSTRACT: Solution-processed organic semiconductor thin films with high charge carrier mobility are necessary for development of next-generation electronic applications, but the rapid processing speed demanded for the industrial-scale production of these thin films poses a challenge to control of their thin-film properties, such as crystallinity, morphology, and film-to-film uniformity. Here, we show a new solution coating method that is compatible with a roll-to-roll printing process at a rate of 2 mm s^{-1} by using a gap-controllable wire bar, motion-programming strategy, and blended active inks. We demonstrate that the coating bar, the horizontal motion of which is repeatedly brought to an intermittent standstill, results in an improved vertically self-stratified structure and a high crystallinity for organic active inks comprising a semiconducting small molecule and a semiconducting polymer. Furthermore, organic transistors prepared by the developed method show superior hole mobility with high operational stability (hysteresis and kink-free transfer characteristics), high uniformity over a large area of a 4 in. wafer, good reproducibility, and superior electromechanical stabilities on a flexible plastic substrate. The bar-coating approach demonstrated here will be a step toward developing industrial-scale practical organic electronics applications.

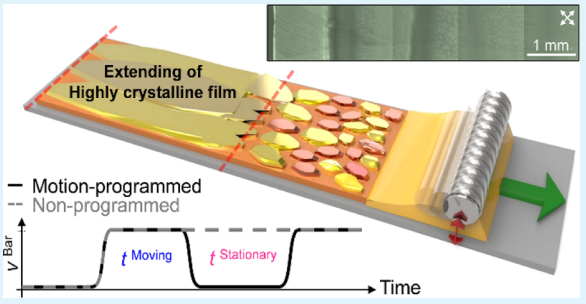

KEYWORDS: *bar coating, organic semiconductors, vertical phase separation, charge transport, organic transistors*

INTRODUCTION

Organic thin film transistors (OTFTs) have received enormous interest due to their great potential for realizing low-cost, lightweight, and flexible electronics that are solution-processed in a large area.[1−8] Recent research efforts in this area have mainly been devoted to developing new organic semiconductor materials with high charge carrier mobility (>10 cm^2 V^{-1} s^{-1}) and devising novel solution-processing techniques that are able to solve the troublesome cost issue of vacuum deposition methods. In the current statues, however, most of the reported solution-processed OTFTs have still been far from their commercial use because of the relatively low charge carrier mobilities and low tolerance to environmental and bias-stress compared with their inorganic counterparts. Furthermore, fabrication of organic semiconductor (OSC) films with high molecular order and preferred molecular orientation, i.e., critical elements in the performance of OTFTs, still remains a challenging work with the current solution-processing technologies.[2,9−12] Some breakthroughs have been made by using soluble small-molecule semiconductor materials, such as triisopropylsilyl pentacene (TIPS-pentacene), 2,8-difluoro-5,11-bis(triethylsilylethynyl) anthradithiophene (diF-TESADT), and 2,7-dioctyl [1]-benzothieno [3,2-*b*][1]benzothiophene (C_8-BTBT). These materials have strong $\pi-\pi$ interaction which enables molecules to be packed in a highly ordered state, exhibiting superior charge carrier transport. Unfortunately, the strong molecular interactions and low viscosity itself lead to a strong propensity to easily dewet on common surfaces and result in discontinuous film morphology that is unfavorable for charge carrier transport.

The development of a reliable solution-phase deposition method is a prerequisite to mass production of OTFT devices based on OSC inks.[13−16] Spin-coating has been frequently

Received: September 19, 2019
Accepted: November 25, 2019
Published: November 25, 2019

DOI: 10.1021/acsami.9b17044
ACS Appl. Mater. Interfaces 2019, 11, 47153−47161

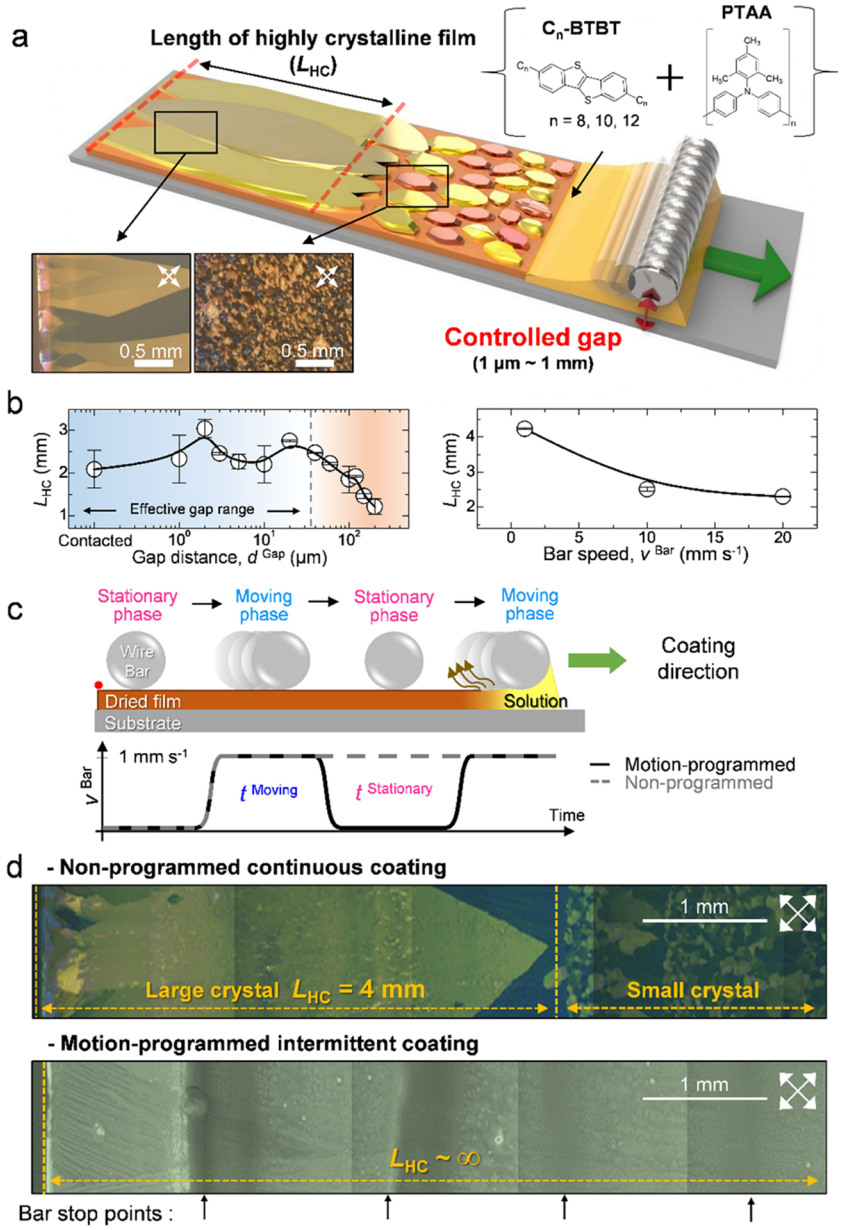

Figure 1. Wire-bar coating method with a controllable gap and a motion-programming strategy. (a) Schematic illustration of the bar-coating process with a gap. The insets in the upper row show the chemical structures of C_n-BTBT and PTAA. The insets in the lower row exhibit the POM of the bar-coated C_8-BTBT:PTAA films. (b) The length of the continuous C_8-BTBT crystalline region (L_{HC}) as a function of the gap distance (d^{Gap}) and bar speed (v^{Bar}). (c) Schematic drawing showing the motion-programmed method. (d) The POM images of bar-coated C_8-BTBT:PTAA films with and without using a motion-programmed wire-bar coating; the images were prepared by attaching separately taken POM images.

used on a lab scale due to its simplicity but it has fatal drawbacks, such as a large amount of material waste, difficulty in scaling up, and incompatibility with a conventional roll-to-roll system. Among various alternative solution processes, bar-coating methods have the advantages of a high deposition rate, roll-to-roll compatibility, and excellent uniformity over a large area.[15,17] In the typical bar-coating process, a film is deposited on an arbitrary substrate by the horizontal continuous movement of a coating bar that is positioned just on the substrate. During bar-coating of a film, a surface of the flexible substrates with prepatterned electrodes would get hurt easily because of the intimate contact made between the coating bar and substrates. The presence of a constant small gap between them, therefore, is necessary for high-throughput reliable fabrication of bar-coated soft electronic devices, and this new-type coating method is attracting much attention as an emerging technique.[18,19]

The presence of a gap at the deposition stage often leads to more highly crystalline films compared with the case where there is no gap. The advantage is likely to mainly come from an enhanced convective mass flow inside the solution, which is driven by the capillary force at the gap. This gap-induced crystallization phenomenon has been found not only in bar coating but also in blade coating, zone-casting, and solution-shearing methods, but the effect of a gap distance (d^{gap}) on the formation of organic crystals has not been studied in detail.[20−23] Moreover, many solution-processing systems use blended inks consisting of small molecule and polymer,[9,24,25]

DOI: 10.1021/acsami.9b17044
ACS Appl. Mater. Interfaces 2019, 11, 47153−47161

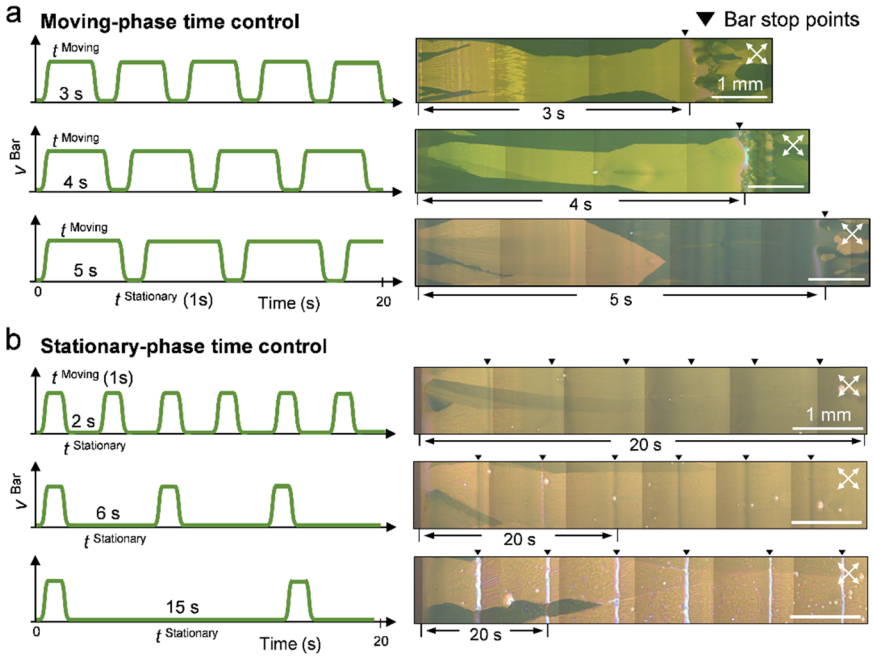

Figure 2. Effects of the bar-motion programming. (a) The POM images of bar-coated C_8-BTBT:PTAA films prepared by using different times of the moving phase (t^{moving} = 3, 4, and 5 s), and (b) different times of the stationary phase ($t^{stationary}$ = 2, 6, and 15 s).

which complicates a proper analysis of such gap-existing coating methods and the understanding of phase separation phenomena therein is yet in its infancy.

Here, we propose a new approach for preparing a large-area uniform highly crystalline OSC thin film using a gap-controlled and motion-programmed bar-coating method and blended inks; our method uses the coating bar, the horizontal motion of which is repeatedly brought to an intermittent standstill for improving the film qualities. Our systematic study based on both computational fluid dynamics simulations and experimental results would give a solution to the critical problems in mass production of organic electronic devices and provide deeper understanding on phase separation and crystallization of organic molecules in our practical method.

RESULTS AND DISCUSSION

Gap-Controlled Bar-Coating Process. The gap-controlled bar-coating process is depicted schematically in Figure 1a. In the system, it includes four major steps: (i) positioning of a fixed coating bar and a substrate (2 × 2 cm^2) on a moving stage, (ii) dispensing a small amount of a semiconductor solution (~60 μL) just in front of the coating bar, (iii) wetting of the solution onto the substrate by horizontal movement of the stage at a constant velocity, and (iv) gradual drying of the wet film. A d^{gap} between the bar and substrate was elaborately controlled from 1 μm to 1 mm by using a motorized positioning system equipped with two laser alignment sensors (Figure S1). The ink solution consists of two OSCs, highly crystalline small molecule and amorphous polymer (see the differential scanning calorimeter curves in Figure S2), i.e., 2,7-alkyl[1]benzothieno[3,2-*b*][1]benzothiophene (C_n-BTBT; n = 8, 10, or 12) and poly[bis(4-phenyl)(2,4,6-trimethylphenyl)-amine] (PTAA). The coating method and preparation of the solution and substrate are provided in detail in the Experimental section, and the overall process is displayed in a video clip available in the Supporting Information (Movie S1).

All printed OSC films were characterized by polarized optical microscopy (POM), and we found out the presence of coexisting large-sized and small-sized C_8-BTBT crystals on the substrate (inset of Figures 1a and S3). The millimeter-scale large-sized C_8-BTBT crystals on par with single-crystalline characteristics along the coating direction were grown continuously from the starting line of the coating bar possibly due to a pinned contact line of the bar. By contrast, the remaining part of the coated film showed only crystals of micrometer-scale small grains, i.e., low-crystalline regions. We quantified the crystal lengths of the front-end highly crystalline film (L^{HC}) that was formed at an initial stage of bar movement and found that L^{HC}s were strongly affected by the processing parameters, d^{gap} and bar speed (v^{bar}). The slower the coating in the smaller gap, the longer the highly crystalline films at the front end of substrates were formed (Figure 1b); this front-end effect was held at the d^{gap} of up to approximately 50 μm, and the C_8-BTBT crystals with the maximum size of 4 mm were obtained at d^{gap} = 2 μm and v^{bar} = 1 mm s^{-1}; the drying behavior at the different gap distances is displayed in a video clip available in the Supporting Information (Movie S2).

Motion-Programmed Bar Coating. Motivated by the front-end effect of the gap, we devised a new coating strategy by programming the dynamic motion of a coating bar to increase L^{HC} further. To maximize the front-end effect, we intentionally brought the coating bar to an intermittent standstill repeatedly (Figure 1c); the moving bar was briefly paused before reaching L^{HC} of the corresponding coating condition. Surprisingly, the C_8-BTBT/PTAA film deposited from the motion-programmed method showed an infinitely continuous highly crystalline film (Figure 1d). In addition, our proposed process could be easily extended to different bimolecular blend systems, such as C_{10}-BTBT/PTAA, C_{12}-BTBT/PTAA, and 2,8-difluoro-5,11-bis(triethylsilylethynyl) anthradithiophene (diF-TESADT)/PTAA (Figure S4). Next, we observed the time effects over the moving phase (t^{moving}) and stationary phase ($t^{stationary}$) on film morphologies at the

DOI: 10.1021/acsami.9b17044
ACS Appl. Mater. Interfaces 2019, 11, 47153−47161

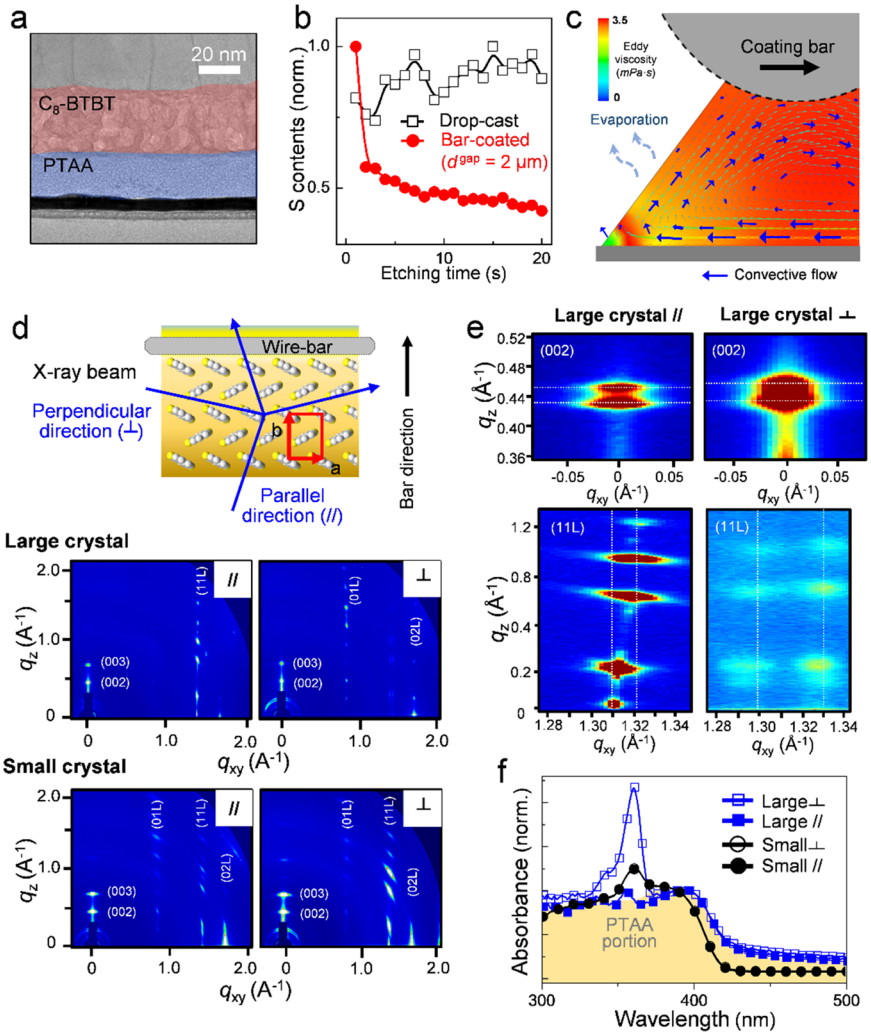

Figure 3. Vertical phase separation and microstructure of bar-coated C_8-BTBT:PTAA thin films. (a) TEM image of the vertically separated bilayer structure (top: C_8-BTBT, bottom: PTAA). (b) XPS depth profiles of sulfur (S) atoms for the films fabricated by drop-casting and bar coating methods. (c) The computational fluid dynamics (CFD) simulation result showing the distribution of solvent flow and eddy viscosity during the coating process (d^{gap} = 10 μm and v^{bar} = 1 mm s^{-1}). (d) 2D-GIXD patterns of the bar-coated C_8-BTBT:PTAA films with different sizes of crystalline domains; the 2D-GIXD images were measured along the parallel (//) or perpendicular directions (⊥) with respect to the bar moving direction. (e) The magnified 2D-GIXD patterns showing the difference between the equilibrium phase and polymorphic phase; (top) the (002) peaks ($q_z^{equilibruim}$ = 0.43 $Å^{-1}$ and $q_z^{polymorph}$ = 0.45 $Å^{-1}$) and (bottom) the (11L) peaks $q_{xy}^{equilibruim}$ = 1.31 $Å^{-1}$ and $q_{xy}^{polymorph}$ = 1.34 $Å^{-1}$). (f) Polarized UV−visible spectra of bar-coated C_8-BTBT:PTAA films with different domain sizes.

processing condition of d^{gap} = 2 μm, v^{bar} = 1 mm s^{-1} (Figure 2a,b). When t^{moving} increased from 3 to 5 s, C_8-BTBT/PTAA films with L^{HC} = ∼3 mm were formed similarly. On the other hand, continuous highly crystalline films were obtained with thick stripes when $t^{stationary}$ increased from 2 to 15 s. The height of stripes increased from ∼5 nm (at $t^{stationary}$ = 2 s) to 175 nm (at $t^{stationary}$ = 15 s) and the locations of the thick stipes were identical with the positions where a coating bar had stopped (Figure S5). These results indicate that the stripes are formed during the stationary phase and the coating bar should be stopped before reaching the length of L^{HC} at the corresponding processing condition and continuously moved to deposit a continuously connected high crystalline film with few grain boundaries. These results provide insightful guidelines for achieving high-quality OSC films at a fast coating rate compatible with a roll-to-roll process when using our motion-programmed gap-controlled bar-coating method.

The formation of the continuous crystalline film can be explained in terms of a stick-and-slip phenomenon during the drying process of the wet films.[13,26] Continuous large crystal growth should have a limited number of nucleation sites. The presence of a wire bar near growing crystals would suppress additional nucleation of OSC molecules in a solution medium (i.e., slip) due to occurrence of a capillary flow beneath the bar and make solute molecules only attached to growing crystals with an aligned direction (i.e., stick) because of thermodynamic preference to homocrystal facets. Especially, the stationary phase inserted between the bar-coating steps would not allow growth of new nuclei that may form inside a bulk solution but make them continuously stick to form an infinitely continuous crystalline film. In striking contrast to our developed method, the conventional bar coating uses a continuously moving wire bar regardless of solvent evaporation and the crystal growth rate so that the absence of a bar near the crystallization zone would have molecules slip from growing crystals and occur in the new grain boundary after L^{HC}.[27]

Gap-Induced Vertical Phase Separation. A vertical structure of the bar-coated C_8-BTBT/PTAA film along the

DOI: 10.1021/acsami.9b17044
ACS Appl. Mater. Interfaces 2019, 11, 47153−47161

out-of-plane direction was investigated using cross-sectional transmission electron microscopy (TEM) and X-ray photoelectron spectroscopy (XPS) combined with Ar^+-ion etching. The TEM image showed a vertically stratified structure with a C_8-BTBT upper layer (~30 nm in thickness) and PTAA on the lower part (~20 nm in thickness), which would be ideal for an active layer of top-gate OTFTs (Figure 3a). The depth profiles of sulfur (S) atoms inside the film also supported the bilayer structure (Figure 3b). Interestingly, the vertical distribution of S atoms was found to be nearly constant when the film was prepared by drop casting of the same C_8-BTBT/PTAA solution, indicating that a small gap between a coating bar and substrates is a necessary condition to effectively induce the vertical phase separation even though the thermodynamic properties of the materials, such as the solubility parameter and surface energy differences, are adequate to provide a strong driving force for vertical phase separation (Tables S1 and S2).[28]

We insist that the gap of a small d^{gap} gives rise to better vertical phase separation in terms of the flow-induced liquid−liquid phase separation and thus leads to efficient and refined crystallization of C_8-BTBT molecules without disturbance but rather help from the PTAA chains (Figure S6). Just after dispensing, C_8-BTBT molecules and PTAA chains would be dispersed homogeneously in the solution. The solution is readily sucked into the gap and forms a thin wet film accompanying a mass flow beneath the wire bar. At that moment, the concentration of the blend solution starts to sharply increase through solvent evaporation and the spacing of the solutes would become closer and easier to interact with each other. C_8-BTBT and PTAA have different solubility parameters of 16.6 and 23.1 $MPa^{1/2}$, respectively (Table S1), which indicates that the mixed phase is thermodynamically unstable and the two materials will be separated. Because of lower surface energy of C_8-BTBT than PTAA (Table S2), the PTAA chains would tend to be aggregated and directed to the lower layer, while the C_8-BTBT molecules would be likely to be directed to the upper layer to form crystals. Given the XPS depth profiling result (Figure 3b), the presence of the narrow gap should enhance the vertical phase separation. Moreover, the amorphousness of a binder polymer (PTAA) is another important factor to enable the phase separation efficiently, showing clear morphologies without any grain boundary at POM images (Figure S7). In practice, the simultaneous crystallization of semicrystalline polymer, i.e., poly(3-hexyl thiophene) (P3HT), was found to prevent C_8-BTBT molecules from packing with each other, inducing randomly mixed structures even at the optimized processing condition.[29]

The presence of the narrow gap beneath a coating bar and the evaporation of the solvent should induce a strong mass flow inside the solution. This gap-induced flow would drive the lower viscosity C_8-BTBT toward the surface and higher viscosity PTAA toward the substrate, resulting in an improved liquid−liquid phase separation behavior and thus contributing to highly crystallized films. To support the proposed mechanism, we calculated the solvent flow at the gap by using the computational fluid dynamics (CFD) simulation. To this end, the experimental condition was simplified using a 2D circular-cut triangle geometry filled only with chlorobenzene solvent. From the computational results, we found two important features. First, the local velocity of the solvent flow is mostly faster as the d^{gap} is smaller and v^{bar} is slower, which matches well with the experimental results (Figure 1b) and supports the flow-induced phase separation at the gap. Second, the zone with high local eddy viscosity, referring to how turbulent the liquid is, exists and could account for the crystallization behavior of C_8-BTBT molecules (Figures 3c and S8). At the small gap distance of 10 μm in the simulation, there exists the high local eddy viscosity zone at the down-left corner whose value is twice higher than the rest of parts. The high viscosity zone could be depicted as the front end of solution droplet being drowned by a coating bar and corresponds to an air−solution−substrate interface. The higher the eddy viscosity, the more active is the turbulence, which indicates that there would be faster evaporation of solvents thereat. This in turn would make a local highly concentrated liquid phase that promotes crystallization of C_8-BTBT. In contrast, there was a high eddy viscosity zone in the interior of the solution when d^{gap} = 400 μm. The C_8-BTBT in the solution center does not contact with air−solution boundaries, so there is no fast evaporation of solvent with active turbulence, and thus this area is rarely suitable for liquid−liquid separation. Interestingly, when d^{gap} = 200 μm, the high eddy viscosity zone could exist only if a bar (or a substrate) moves as slow as v^{bar} = 1 mm s^{-1} (Figure S8).

Crystalline Characteristics of Bar-Coated Films. Two-dimensional grazing incidence X-ray diffraction (2D-GIXD) experiments were performed to verify crystalline characteristics of the two different bar-coated C_8-BTBT/PTAA thin films with large-sized and small-sized crystals. The 2D-GIXD patterns were measured along both directions parallel and perpendicular to the bar-moving direction, respectively, and exhibited different features, which indicates that the films have an anisotropic in-plane structure (Figure 3d); the difference was predominant in the film with large-sized crystals, and the coating direction corresponds to *b*-axis in the unit cell of C_8-BTBT, i.e., parallel to the bar-coating direction. The two films showed many well-defined reflection spots along the q_z axis at a given q_{xy}, indicating well-ordered 3D crystalline structures. The distinct (00*l*) reflections represent along the out-of-plane directions, showing that the C_8-BTBT crystals adopted a standing-up structure on the substrates. The full width at half-maximum (FWHM) values of the (002) peaks and FWHMs in the pole figures at the peaks were found to be much larger for the small crystal film than the large crystal film (Figure S9).[30] These results demonstrate the superior molecular order in the large crystal C_8-BTBT/PTAA film deposited by our proposed bar-coating method.

More importantly, the existence of a polymorph was confirmed by the presence of additional diffraction peaks near (002) peaks in the out-of-plane direction and near the (11L) Bragg rods in the in-plane direction (Figure 3e). The (002) peak shifted from q_z = 0.43 $Å^{-1}$ (equilibrium) to 0.45 $Å^{-1}$ (polymorph), and the (11L) Bragg rod also did from q_{xy} = 1.32 $Å^{-1}$ (equilibrium) to 1.34 $Å^{-1}$ (polymorph) (see the magnified peaks of the small crystal samples in Figure 3e and the summary in Table S3). These results indicate collapsing of the unit cell, possibly due to the large strain arisen from the fast mass flow during the bar-coating process. This trend was more distinct when the sample was measured along the perpendicular direction, which means that the large strain resulting from the mass flow largely affected the molecular packing along the *b*-axis direction, macroscopically the coating bar direction. The densified molecular packing would accompany a smaller intermolecular spacing and $\pi-\pi$ stacking distance closer than that of the equilibrium molecular packing. Bao and co-workers

DOI: 10.1021/acsami.9b17044
ACS Appl. Mater. Interfaces 2019, 11, 47153−47161

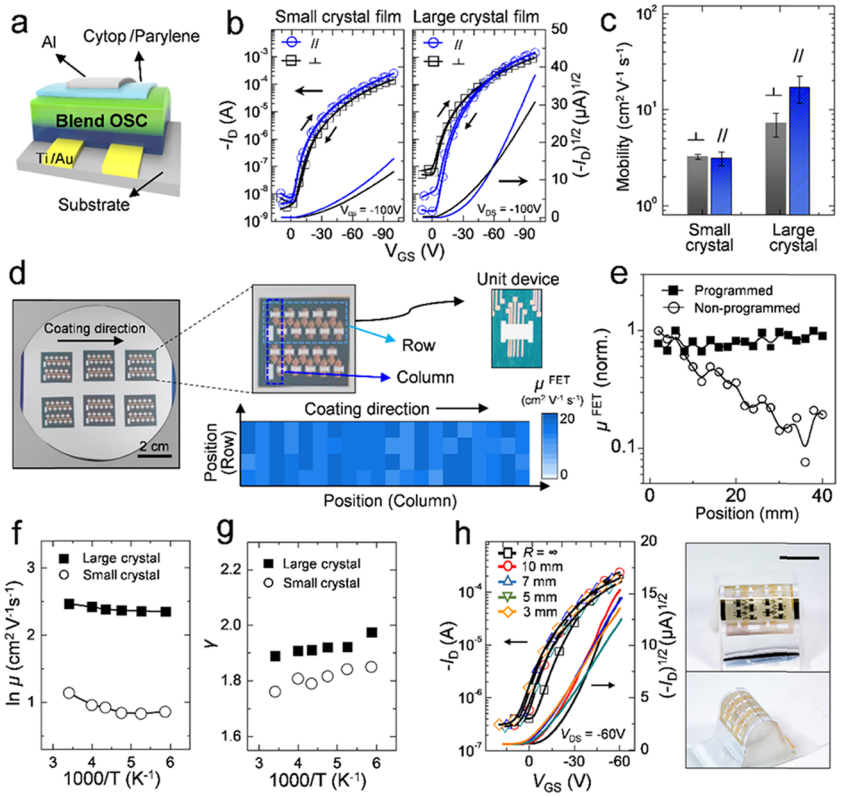

Figure 4. Electrical characteristics of bar-coated organic semiconductor thin films and flexible devices. (a) Schematic illustration of OTFT structure. (b) Transfer characteristics and (c) the summary of device performances for the OTFT devices prepared with the bar-coated C_8-BTBT:PTAA films. (d) Photographic image and mobility uniformity map for OTFT arrays prepared on a 4 in. SiO_2/Si wafer. (e) Uniformity comparison in terms of μ_{FET} values. (f) Field-effect mobilities (μ_{FET}), and (g) fitting parameter γ (γ) as a function of T. (h) Transfer curves and photographic images (scale bar, 1 cm) of flexible OTFTs prepared on a transparent polymer substrate. The curves were measured at flat or bended states with different bending radii (R = 3, 5, 7, and 10 mm).

have observed the similar polymorphism in the C_8-BTBT/polystyrene film deposited by the off-centered spin-coating method.[10]

Furthermore, polarized UV−vis spectra verified again the anisotropic structure of the C_n-BTBT/PTAA film with large-sized crystals that had a strong peak at 360 nm, assigned to the π−π* transition of the BTBT conjugated core (Figures 3f and S10).[31] The film showed the dichroic ratio ($A_\perp/A_{//}$ at 361 nm) of 2.4. Since the transition dipole lies perpendicular to the backbone structure, the BTBT backbones in the polymorph would be aligned more closely to the perpendicular direction to the bar-moving direction (and the b-axis direction in the equilibrium structure). Such molecular alignment was found to be similar in other bimolecular systems deposited by our bar-coating method (Figure S10). By contrast, the small crystal films showed only a small peak at 360 nm without a preferred in-plane orientation.

Electrical Properties of OTFTs. Electrical characteristics of the bar-coated C_8-BTBT/PTAA film were studied by fabricating and analyzing the OTFT devices prepared with the film. The blend film was bar-coated onto the substrate with prepatterned Ti/Au source/drain electrodes, followed by spin-coated Cytop and thermally evaporated parylene layers as a dual gate dielectric (Figures 4a and S11). The ultrathin Cytop interlayer reduces interfacial traps at the OSC layers and often makes low off-current (Figure S12).[32] As mentioned above, the vertically stratified structure consisting of a C_8-BTBT (top)/PTAA (bottom) bilayer takes an advantage in top-gate OTFTs where the charge carrier pathway forms in the top C_8-BTBT layer. The top-contact bottom-gate OTFT devices with the same film showed poor device performances because of the formation of the channel at the buried amorphous PTAA layer (Figure S13).[33] By contrast, the best bottom-contact top-gate C_8-BTBT/PTAA OTFTs exhibited high hole mobilities of up to 20 cm^2 V^{-1} s^{-1} with an on/off ratio of ~10^7 when measured along the bar coating direction (Figure 4b, Figure S14 and Table S4); the C_{10}-BTBT/PTAA and C_{12}-BTBT/PTAA-based devices showed mobilities approaching 20 cm^2 V^{-1} s^{-1} and the diF-TESADT/PTAA film also did over 10 cm^2 V^{-1} s^{-1} (Figure S15 and Table S4). These values are much higher than those of C_n-BTBT TFTs fabricated with spin-coating or thermal evaporation methods.[34,35] The mobility values were measured in vacuum, and they were about 16% higher than the values measured in air. Moreover, the C_8-BTBT/PTAA films with large crystals showed anisotropic charge carrier mobility values (Figure 4c, the mobility anisotropy of 2.4), possibly resulting from the anisotropic crystalline structure. The prepared OTFT devices mostly showed excellent electrical characteristics, especially for kink-and-hysteresis-free transfer curves with the saturated transconductance within the wide range of V_G (Figure S16). Although the superior crystalline structure would be the primary factor for explaining the very high hole mobility, the PTAA bottom layer was also shown to be useful for lowering the charge injection barrier by forming the cascade energy structure (Figure S17).[36] The contact resistance estimated by the Y-function method was largely reduced from 2908 Ω cm (for OTFT prepared with homo C_8-BTBT films) to 1474 Ω cm (for the device with the blend film;

DOI: 10.1021/acsami.9b17044
ACS Appl. Mater. Interfaces 2019, 11, 47153−47161

Figure S18).[37] Furthermore, the bar-coated devices showed excellent device-to-device uniformity and long-term environmental stability as well. We fabricated an array of OTFT devices on a 4 in. wafer (Figure 4d,e), which yielded the standard error of only 5% in mobility values and operated for more than 20 days without severe degradation even though the devices had no encapsulation layers (Figure S19), to the best of our knowledge, which are the best results given that the coating rate, deposition, and electrical properties are considered together (Table S5). These results would demonstrate the capability of our coating method to industry-scale production of high-quality OSC films.

Charge Transport Mechanism. To identify differences in the charge transport mechanisms in the bar-coated C_8-BTBT/PTAA film with large-sized and small-sized crystals, we conducted TFT measurements at a temperature ranging from 170 to 293 K (Figure 4f).[38] The measured mobilities showed far weak temperature dependence for both samples. The activation energy estimated from the slopes was twice smaller for large-sized crystal film (5.5 meV) than small-sized crystal (9.5 meV), which would be attributable to fewer grain boundaries disturbing the charges transporting (Figure S20).[39] The two absolute values of the activation energy are much smaller than the thermal energy at room temperature (~25 meV), suggesting that the actual transport mechanism might be an intermediate regime between the bandlike and hopping transport.[40] The series of transfer curves were fitted to $I_D \propto (V_G - V_{th})^{\gamma}$, which gave the exponent γ (Figure 4g). For the large crystal sample, the value was the nearly temperature-independent value of 1.9, close to the ideal value of 2, indicating a very low degree of disorder in our bar-coated C_8-BTBT/PTAA film with large crystals and also implying the intermediate charge transport regime; the small crystal films showed a bit smaller γ value of 1.8.

Flexible OTFT Array. To demonstrate that our bar-coating method has high compatibility with flexible organic electronics, bar-coated OTFT devices were fabricated on 125 μm thick flexible polyethylene naphthalate (PEN) substrates with the same device fabrication steps.[41] In addition, we examined their electromechanical stability under bending stress of the bending radius of 3, 5, 7, and 10 mm, where the bending radius of 3 mm corresponded to the maximum strain of 2.1% (Figure 4h). The devices operated very well and showed only slight differences in the transfer curves while bending; change of performance parameters are provided in the Supporting Information (Figure S21). The electromechanical stability of the devices is attributed to the use of a binder polymer, PTAA herein, as well as thinness (~20 nm) of the highly crystalline C_8-BTBT layer.

CONCLUSIONS

We introduced the novel approach to deposit high-quality OSC thin films using a gap-controlled motion-programmed bar coating method and blend OSC inks. Careful adjustment of processing parameters, d^{gap} and v^{bar}, was found to lengthen the crystalline region at the film's front end, and the front-end effect was maximized by programming the dynamic motion of a coating bar to be repeatedly brought to an intermittent standstill. The resulting continuously connected highly crystalline C_8-BTBT/PTAA thin film showed the ideally self-stratified bilayer structure, and thus the flow-induced liquid–liquid phase separation at the gap was proposed as a plausible mechanism. Anisotropic crystalline structure and presence of a polymorph that has a densified unit cell were experimentally verified, and the strained microstructure yielded superior electrical properties with high uniformity. Our proposed method deposits high-quality OSC thin films at a high speed in a scalable way. We believe that this method is compatible with roll-to-roll systems for mass production, and it would be able to contribute to commercialization of the next-generation electronics based on organic materials.

EXPERIMENTAL SECTION

Materials. C_8-BTBT, PTAA, diF-TESADT, and 1-chlorobenzene (CB, anhydrous) were purchased from Sigma-Aldrich Co. C_{10}-BTBT and C_{12}-BTBT were synthesized according to the established procedures.[34] Cytop and Parylene-C were purchased from Bellex International Co. and KISCO Ltd., respectively. All purchased materials were used as received.

Ink Formulation and Bar-Coating Procedure. The highest device performances were achieved with the blend solutions at a concentration of 20 mg mL^{-1} and at a weight ratio of 3:4 C_8-BTBT:PTAA in a CB solution. The other solutions blended with PTAA were prepared at a concentration of 20 mg mL^{-1} for diF-TESADT, 15 mg mL^{-1} for C_{10}-BTBT, and 10 mg mL^{-1} for C_{12}-BTBT at a weight ratio of 3:4. Before dispensing ink, a wire bar (a wire distance of 60 μm) was fixed at the bar coater (Printed Electro Mechanical System, PEMS), which was equipped with a two-axis motorized positioning system, plate heating system, and layer sensors for gap control. The coating was proceeded by moving the stage with the speed of 1–20 mm s^{-1} after dispensing 60 μL of the solution to the coating direction side of the bar on the 30 °C heated stage. The gap between the bar and the substrate was carefully adjusted with 1 μm accuracy.

Fabrication of OTFT. A 300 nm thick thermally grown SiO_2/Si wafer or 125 μm thick flexible plastic film (PEN, Tenjin Dupont) served as a substrate after sequential cleansing in an ultrasonic bath with deionized water, acetone, isopropanol, and ethanol for 10 min each. The source/drain electrodes (Ti 5 nm, Au 20 nm) were thermally evaporated (rate of 3–5 Å s^{-1}) through a shadow mask defining channel lengths (50, 100, 150, and 200 μm) and width (1000 μm). Prior to bar-coating, the substrates were exposed to the ultraviolet ozone cleaner (AH1700, Ahtech LTS) for 15 min. The formulated inks were deposited onto the pretreated substrates using the wire-bar coater. The optimized conditions for devices were the gap distance of 2 μm and the bar speed of 1 mm s^{-1}. Cytop diluted with CT180 solvent (a volume ratio of 1:5) was spin-coated above the semiconductor films, and 500 nm thick Parylene-C was vacuum-deposited by the Parylene coater (OBTPC 500, Obang Technology). The Al gate electrodes (40 nm thick) were thermally evaporated through a shadow mask.

Characterization. The crystalline characteristics of small molecule films was visualized using polarized optical microscopy (Eclipse 80i, Nikon and Carl Zeiss), and the morphology of films were collected in the tapping mode by atomic force microscopy (AFM, Digital Instruments Multimode). 2D-GIXD measurements were performed using the synchrotron source at the 3C and 9A beamlines at the Pohang Accelerator Laboratory (PAL) in Korea. The cross-sectional image of the vertically stratified bilayer structure was analyzed by transmission electron microscopy (Jeol, JEM-2200FS). An X-ray photoelectron spectrometer (XPS, ESCALAB 250Xi) with Ar-ion source etching the films (2 kV, 2 × 2 mm^2) were used for depth profiling. Polarized UV–vis absorption spectra were obtained using a UV–vis spectrophotometer (CARY-5000, Varian). The surface and film thickness were analyzed by a Contact Surface profilometer (NanoMap-PS, HTSK). The electrical characteristics of the OTFTs were measured using a Keithley 4200-SCS semiconductor parametric analyzer at a typical temperature in a vacuum chamber. The field-effect mobility (μ_{FET}) and the threshold voltage (V_{th}) were estimated in the saturation regime (V_{DS} = −60 or −100 V) using the following equation

DOI: 10.1021/acsami.9b17044
ACS Appl. Mater. Interfaces 2019, 11, 47153–47161

$$I_D = \frac{W}{2L}\mu_{FET}C_i(V_{GS} - V_{th})^2 \quad (1)$$

where I_D is the drain current, C_i is the unit capacitance of the gate dielectric, V_{GS} is the gate-source voltage, W is the channel width, and L is the channel length. The capacitance−voltage curves were measured using a semiconductor analyzer (Agilent 4156C) and an LCR meter (E4980A) in an ambient environment.

Computational Method. Computational fluid dynamics (CFD) modeling was implemented to figure out how a solvent theprocedure of crystallization microscopically. The standard $k - \varepsilon$ model was used for the turbulence conditions. Boundary conditions were set at the air, metal, and substrate interfaces. General equations for the system conservation are included and were solved numerically using the ANSYS 17.2 program with Fluent 17.2.0 when the system reaches the steady state.

■ ASSOCIATED CONTENT

Supporting Information

The Supporting Information is available free of charge at https://pubs.acs.org/doi/10.1021/acsami.9b17044.

Wire-bar coater, differential scanning calorimeter, polarized optical microscope images, α-step, atomic force microscopy, computational fluid dynamics simulation, pole figures and full width at half maximum at (002), polarized UV−vis spectroscopy, capacitance of dielectric, transfer curves of Cytop device, TCBG device, $C_{10,12}$-BTBT and diF-TESADT, output curve and transconductance, energy level, contact resistance, environmental stability, activation plot of mobility, solubility parameter, surface tension, crystallographic information of C8-BTBT/PTAA films, and electrical performances of various films (PDF)

Movie videos of bar coating and crystal growth (AVI) (AVI)

■ AUTHOR INFORMATION

Corresponding Author

*E-mail: kwcho@postech.ac.kr.

ORCID

Boseok Kang: 0000-0003-4295-3881

Won Bo Lee: 0000-0001-7801-083X

Kilwon Cho: 0000-0003-0321-3629

Author Contributions

‖S.B.L. and B.K. contributed equally to this work.

Notes

The authors declare no competing financial interest.

■ ACKNOWLEDGMENTS

This work was supported by the Center for Advanced Soft-Electronics funded by the Ministry of Science and ICT as Global Frontier Project (Code no. 2011-0031628). Portions of this research were carried out at the 3C, 4D, 5A, 8A2, 9A, and 10A2 beam lines of the Pohang Accelerator Laboratory, Korea.

■ REFERENCES

(1) Minemawari, H.; Yamada, T.; Matsui, H.; Tsutsumi, J.; Haas, S.; Chiba, R.; Kumai, R.; Hasegawa, T. Inkjet Printing of Single-Crystal Films. *Nature* **2011**, *475*, 364−367.

(2) Paterson, A. F.; Treat, N. D.; Zhang, W.; Fei, Z.; Wyatt-Moon, G.; Faber, H.; Vourlias, G.; Patsalas, P. A.; Solomeshch, O.; Tessler, N.; Heeney, M.; Anthopoulos, T. D. Small Molecule/Polymer Blend Organic Transistors with Hole Mobility Exceeding 13 cm^2 V^{-1} S^{-1}. *Adv. Mater.* **2016**, *28*, 7791−7798.

(3) Kang, B.; Lee, S. K.; Jung, J.; Joe, M.; Lee, S. B.; Kim, J.; Lee, C.; Cho, K. Nanopatched Graphene with Molecular Self-Assembly toward Graphene-Organic Hybrid Soft Electronics. *Adv. Mater.* **2018**, *30*, 1706480−1706489.

(4) Zhao, Y.; Di, C. A.; Gao, X.; Hu, Y.; Guo, Y.; Zhang, L.; Liu, Y.; Wang, J.; Hu, W.; Zhu, D. All-Solution-Processed, High-Performance n-Channel Organic Transistors and Circuits: Toward Low-Cost Ambient Electronics. *Adv. Mater.* **2011**, *23*, 2448−2453.

(5) Kuribara, K.; Wang, H.; Uchiyama, N.; Fukuda, K.; Yokota, T.; Zschieschang, U.; Jaye, C.; Fischer, D.; Klauk, H.; Yamamoto, T.; Takimiya, K.; Ikeda, M.; Kuwabara, H.; Sekitani, T.; Loo, Y. L.; Someya, T. Organic Transistors with High Thermal Stability for Medical Applications. *Nat. Commun.* **2012**, *3*, 723−729.

(6) Lee, J. H.; Park, Y. S.; Cho, S.; Kang, I. S.; Kim, J. K.; Jeong, U. Output Voltage Modulation in Triboelectric Nanogenerator by Printed Ion Gel Capacitors. *Nano Energy* **2018**, *54*, 367−374.

(7) Yamamura, A.; Watanabe, S.; Uno, M.; Mitani, M.; Mitsui, C.; Tsurumi, J.; Isahaya, N.; Kanaoka, Y.; Okamoto, T.; Takeya, J. Wafer-Scale, Layer-Controlled Organic Single Crystals for High-Speed Circuit Operation. *Sci. Adv.* **2018**, *4*, No. eaao5758.

(8) Kang, B.; Lee, W. H.; Cho, K. Recent Advances in Organic Transistor Printing Processes. *ACS Appl. Mater. Interfaces* **2013**, *5*, 2302−2315.

(9) Lee, W. H.; Kwak, D.; Anthony, J. E.; Lee, H. S.; Choi, H. H.; Kim, D. H.; Lee, S. G.; Cho, K. The Influence of the Solvent Evaporation Rate on the Phase Separation and Electrical Performances of Soluble Acene-Polymer Blend Semiconductors. *Adv. Funct. Mater.* **2012**, *22*, 267−281.

(10) Yuan, Y.; Giri, G.; Ayzner, A. L.; Zoombelt, A. P.; Mannsfeld, S. C.; Chen, J.; Nordlund, D.; Toney, M. F.; Huang, J.; Bao, Z. Ultra-High Mobility Transparent Organic Thin Film Transistors Grown by an Off-Centre Spin-Coating Method. *Nat. Commun.* **2014**, *5*, No. 3005.

(11) Peng, B.; Huang, S.; Zhou, Z.; Chan, P. K. L. Solution-Processed Monolayer Organic Crystals for High-Performance Field-Effect Transistors and Ultrasensitive Gas Sensors. *Adv. Funct. Mater.* **2017**, *27*, 1700999−1701006.

(12) Xue, G.; Wu, J.; Fan, C.; Liu, S.; Huang, Z.; Liu, Y.; Shan, B.; Xin, H. L.; Miao, Q.; Chen, H.; Li, H. Boosting the Electron Mobility of Solution-Grown Organic Single Crystals Via Reducing the Amount of Polar Solvent Residues. *Mater. Horiz.* **2016**, *3*, 119−123.

(13) Soeda, J.; Okamoto, T.; Mitsui, C.; Takeya, J. Stable Growth of Large-Area Single Crystalline Thin Films from an Organic Semiconductor/Polymer Blend Solution for High-Mobility Organic Field-Effect Transistors. *Org. Electron.* **2016**, *39*, 127−132.

(14) Zhang, Z.; Peng, B.; Ji, X.; Pei, K.; Chan, P. K. L. Marangoni-Effect-Assisted Bar-Coating Method for High-Quality Organic Crystals with Compressive and Tensile Strains. *Adv. Funct. Mater.* **2017**, *27*, 1703443−1703451.

(15) Khim, D.; Han, H.; Baeg, K. J.; Kim, J.; Kwak, S. W.; Kim, D. Y.; Noh, Y. Y. Simple Bar-Coating Process for Large-Area, High-Performance Organic Field-Effect Transistors and Ambipolar Complementary Integrated Circuits. *Adv. Mater.* **2013**, *25*, 4302−4308.

(16) Na, J. Y.; Kang, B.; Lee, S. G.; Cho, K.; Park, Y. D. Surface-Mediated Solidification of a Semiconducting Polymer During Time-Controlled Spin-Coating. *ACS Appl. Mater. Interfaces* **2017**, *9*, 9871−9879.

(17) Bucella, S. G.; Luzio, A.; Gann, E.; Thomsen, L.; McNeill, C. R.; Pace, G.; Perinot, A.; Chen, Z.; Facchetti, A.; Caironi, M. Macroscopic and High-Throughput Printing of Aligned Nanostructured Polymer Semiconductors for Mhz Large-Area Electronics. *Nat. Commun.* **2015**, *6*, No. 8394.

(18) del Pozo, F. G.; Fabiano, S.; Pfattner, R.; Georgakopoulos, S.; Galindo, S.; Liu, X.; Braun, S.; Fahlman, M.; Veciana, J.; Rovira, C.; Crispin, X.; Berggren, M.; Mas-Torrent, M. Single Crystal-Like Performance in Solution-Coated Thin-Film Organic Field-Effect Transistors. *Adv. Funct. Mater.* **2016**, *26*, 2379−2386.

DOI: 10.1021/acsami.9b17044
ACS Appl. Mater. Interfaces 2019, 11, 47153−47161

(19) Pitsalidis, C.; Kalfagiannis, N.; Hastas, N. A.; Karagiannidis, P. G.; Kapnopoulos, C.; Ioakeimidis, A.; Logothetidis, S. High Performance Transistors Based on the Controlled Growth of Triisopropylsilylethynyl-Pentacene Crystals via Non-Isotropic Solvent Evaporation. *RSC Adv.* **2014**, *4*, 20804−20813.
(20) Niazi, M. R.; Li, R.; Qiang Li, E.; Kirmani, A. R.; Abdelsamie, M.; Wang, Q.; Pan, W.; Payne, M. M.; Anthony, J. E.; Smilgies, D.-M.; Thoroddsen, S. T.; Giannelis, E. P.; Amassian, A. Solution-Printed Organic Semiconductor Blends Exhibiting Transport Properties on Par with Single Crystals. *Nat. Commun.* **2015**, *6*, No. 8598.
(21) Janneck, R.; Vercesi, F.; Heremans, P.; Genoe, J.; Rolin, C. Predictive Model for the Meniscus-Guided Coating of High-Quality Organic Single-Crystalline Thin Films. *Adv. Mater.* **2016**, *28*, 8007−8013.
(22) Schuettfort, T.; Thomsen, L.; McNeill, C. R. Observation of a Distinct Surface Molecular Orientation in Films of a High Mobility Conjugated Polymer. *J. Am. Chem. Soc.* **2013**, *135*, 1092−1101.
(23) Stolte, M.; Gsanger, M.; Hofmockel, R.; Suraru, S. L.; Wurthner, F. Improved Ambient Operation of n-Channel Organic Transistors of Solution-Sheared Naphthalene Diimide under Bias Stress. *Phys. Chem. Chem. Phys* **2012**, *14*, 14181−14185.
(24) Lee, W. H.; Lim, J. A.; Kwak, D.; Cho, J. H.; Lee, H. S.; Choi, H. H.; Cho, K. Semiconductor-Dielectric Blends: A Facile All Solution Route to Flexible All-Organic Transistors. *Adv. Mater.* **2009**, *21*, 4243−4248.
(25) Li, X.; Smaal, W. T. T.; Kjellander, C.; van der Putten, B.; Gualandris, K.; Smits, E. C. P.; Anthony, J.; Broer, D. J.; Blom, P. W. M.; Genoe, J.; Gelinck, G. Charge Transport in High-Performance Ink-Jet Printed Single-Droplet Organic Transistors Based on a Silylethynyl Substituted Pentacene/Insulating Polymer Blend. *Org. Electron.* **2011**, *12*, 1319−1327.
(26) Huang, J.; Fan, R.; Connor, S.; Yang, P. One-Step Patterning of Aligned Nanowire Arrays by Programmed Dip Coating. *Angew. Chem., Int. Ed. Engl.* **2007**, *46*, 2414−2417.
(27) Born, P.; Blum, S.; Munoz, A.; Kraus, T. Role of the Meniscus Shape in Large-Area Convective Particle Assembly. *Langmuir* **2011**, *27*, 8621−8633.
(28) Kang, B.; Ge, F.; Qiu, L.; Cho, K. Effective Use of Electrically Insulating Units in Organic Semiconductor Thin Films for High-Performance Organic Transistors. *Adv. Electron. Mater.* **2017**, *3*, No. 1600240.
(29) Madec, M.-B.; Crouch, D.; Llorente, G. R.; Whittle, T. J.; Geoghegan, M.; Yeates, S. G. Organic Field Effect Transistors from Ambient Solution Processed Low Molar Mass Semiconductor−Insulator Blends. *J. Mater. Chem.* **2008**, *18*, 3230−3236.
(30) Kang, B.; Park, N.; Lee, J.; Min, H.; Choi, H. H.; Lee, H. S.; Cho, K. Surface-Order Mediated Assembly of Π-Conjugated Molecules on Self-Assembled Monolayers with Controlled Grain Structures. *Chem. Mater.* **2015**, *27*, 4669−4676.
(31) Zhang, F.; Mohammadi, E.; Luo, X.; Strzalka, J.; Mei, J.; Diao, Y. Critical Role of Surface Energy in Guiding Crystallization of Solution-Coated Conjugated Polymer Thin Films. *Langmuir* **2018**, *34*, 1109−1122.
(32) Yoo, H.; Lee, S. B.; Lee, D.-K.; Smits, E. C. P.; Gelinck, G. H.; Cho, K.; Kim, J.-J. Top-Split-Gate Ambipolar Organic Thin-Film Transistors. *Adv. Electron. Mater.* **2018**, *4*, 1700536−1700543.
(33) Zhao, K.; Wodo, O.; Ren, D.; Khan, H. U.; Niazi, M. R.; Hu, H.; Abdelsamie, M.; Li, R.; Li, E. Q.; Yu, L.; Yan, B.; Payne, M. M.; Smith, J.; Anthony, J. E.; Anthopoulos, T. D.; Thoroddsen, S. T.; Ganapathysubramanian, B.; Amassian, A. Vertical Phase Separation in Small Molecule:Polymer Blend Organic Thin Film Transistors Can Be Dynamically Controlled. *Adv. Funct. Mater.* **2016**, *26*, 1737−1746.
(34) Ebata, H.; Izawa, T.; Miyazaki, E.; Takimiya, K.; Ikeda, M.; Kuwabara, H.; Yui, T. Highly Soluble [1]Benzothieno[3,2-*b*]-Benzothiophene (BTBT) Derivatives for High-Performance, Solution-Processed Organic Field-Effect Transistors. *J. Am. Chem. Soc.* **2007**, *129*, 15732−15733.
(35) Ren, H.; Tang, Q.; Tong, Y.; Liu, Y. 320-Nm Flexible Solution-Processed 2,7-Dioctyl[1] Benzothieno[3,2-*b*]Benzothiophene Transistors. *Materials* **2017**, *10*, 918−926.
(36) Horowitz, G. Interface Modification for Tuning the Contact Resistance of Metal/Organic Semiconductor Junctions. *Open Appl. Phys. J.* **2011**, *4*, 2−7.
(37) Xu, Y.; Minari, T.; Tsukagoshi, K.; Chroboczek, J. A.; Ghibaudo, G. Direct Evaluation of Low-Field Mobility and Access Resistance in Pentacene Field-Effect Transistors. *J. Appl. Phys.* **2010**, *107*, 114507−114513.
(38) Venkateshvaran, D.; Nikolka, M.; Sadhanala, A.; Lemaur, V.; Zelazny, M.; Kepa, M.; Hurhangee, M.; Kronemeijer, A. J.; Pecunia, V.; Nasrallah, I.; Romanov, I.; Broch, K.; McCulloch, I.; Emin, D.; Olivier, Y.; Cornil, J.; Beljonne, D.; Sirringhaus, H. Approaching Disorder-Free Transport in High-Mobility Conjugated Polymers. *Nature* **2014**, *515*, 384−388.
(39) Choi, H. H.; Lee, W. H.; Cho, K. Bias-Stress-Induced Charge Trapping at Polymer Chain Ends of Polymer Gate-Dielectrics in Organic Transistors. *Adv. Funct. Mater.* **2012**, *22*, 4833−4839.
(40) He, D.; Qiao, J.; Zhang, L.; Wang, J.; Lan, T.; Qian, J.; Li, Y.; Shi, Y.; Chai, Y.; Lan, W.; Ono, L. K.; Qi, Y.; Xu, J.-B.; Ji, W.; Wang, X. Ultrahigh Mobility and Efficient Charge Injection in Monolayer Organic Thin-Film Transistors on Boron Nitride. *Sci. Adv.* **2017**, *3*, No. e1701186.
(41) Lai, S.; Temiño, I.; Cramer, T.; del Pozo, F. G.; Fraboni, B.; Cosseddu, P.; Bonfiglio, A.; Mas-Torrent, M. Morphology Influence on the Mechanical Stress Response in Bendable Organic Field-Effect Transistors with Solution-Processed Semiconductors. *Adv. Electron. Mater.* **2018**, *4*, 1700271−1700279.

DOI: 10.1021/acsami.9b17044
ACS Appl. Mater. Interfaces 2019, 11, 47153−47161